Light Modulation with Silicon Devices

Andrea Irace[1], Giovanni Breglio[1], Mario Iodice[2], and Antonello Cutolo[3]

[1] University of Naples "*Federico II*",
Department of Electronic and Telecommunication Engineerging,
Via Claudio, 21, 80125 Naples, Italy
{irace,breglio}@diesun.die.unina.it
[2] Istituto per la Microelettronica e Microsistemi – Sezione di Napoli – IMM-CNR,
Via Pietro Castellino, Napoli, Italy
iodice@irece.na.cnr.it
[3] University of Sannio, Corso Garibaldi, Benevento, Italy
cutolo@unisannio.it

Abstract. In this chapter we deal with different approaches to obtain fast and low power consumption amplitude modulation with silicon optoelettronic devices. After a description of the various physical effects that allow the interaction of material modification with travellling light we describe the optical configurations and different driving schemes that, so far, have been presented to the scientific community.

1 Introduction

Among optoelectronic materials, silicon is acquiring more and more importance for the fabrication of photonic integrated circuits. From its initial use as a mere substrate for the realization of silica-based devices, or as a motherboard for the assembly of lasers, photodetectors, and switches, the technologically best-known semiconductor has rapidly attained to the role of an active material. For example, silicon-on-silicon or silicon-on-insulator waveguides have been successfully fabricated, while a wide range of light modulators and switches, exploiting electro-optical, optomechanical, or thermo-optical working principles have been proposed.

Moreover, in the last ten years we are looking at new and very promising *weddings* between standard electronic and different aspects of others fields. In particular, the simultaneous use of electrical and optical signals on the same chip gives us the possibility to realize the so called optoelectronic integrated circuit (OEIC), characterized by high speed, high efficiency and electromagnetic immunity. Since Silicon is the basic material for electronics, in recent times it has been also tested in optoelectronic applications.

Near-infrared ($\lambda > 1.2\,\mu$m) silicon photonic integrated circuits (Si-PICs) have received great interest in the past few years. Even if III–V compounds are the most suitable candidates for fast switching purposes, the wide knowledge of silicon processing technologies makes silicon-based devices very attractive [1].

L. Pavesi, D. J. Lockwood (Eds.): Silicon Photonics, Topics Appl. Phys. **94**, 361–392 (2004)

It is, then, reasonable to foresee that the performance of Si-PICs will eventually surpass that of III–IV PICs in several areas. The principal areas of application of Si-based optoelectronics are wherever a simple low-cost optical device is required and when it is instrumental to realize the optical circuit and the electronic circuit onto the same substrate.

Even though silicon physical properties, such as indirect band-gap and low carrier mobility, may pose some obstacles to the success of optoelectronics circuits and systems, there are several market niches where silicon-based optoelectronics can play a crucial role. The motivation for this new vision have to be found in the need of cheap systems which can be integrated in consumer electronic apparatus, for communication and sensing purposes. In particular, for modulation applications, different configurations of two or three terminal [2] devices based on free carrier absorption [3] or interferometric configurations, such as Fabry–Perot [4] or Mach–Zehnder modulators, have been realized.

With several exceptions therefore most practical modulators are based on a shift in the real or imaginary refractive index of the material in which the optical field propagates. The induced index changes then often lead to variations in macroscopically measurable quantities, usually intensity or direction. We therefore start this chapter from the description of the physical effects that can cause these variations and after we move onto the description of the optical modulation mechanisms and finally the analysis of the most convenient electrical driving schemes.

2 Physical Effects

Since any optical modulator presented in literature is based on charge/field or temperature induced variation of the optical properties of silicon, before entering the details of the optical modulation schemes and the electrical driving options, some attention has to be paid to the physical mechanisms which underly the variation of refractive index and absorption coeffcient in this material.

Even if the totality of the optical modulators are based on carrier-induced or thermo-optical effect, also field-induced variation of refractive index and absorption coefficent will be dealt with since they have been theoretically predicted and experimentally observed.

2.1 Field and Charge-Carrier Effect

The complex refractive index of any material can be written as $n + \mathrm{i}k$ where n is the refractive index and the imaginary part k is the optical extinction coefficient. k is related to α, the linear absorption coefficient, by the relation $k = \alpha\lambda/4\pi$ where λ is the optical wavelength. It is known that n and k are

related by the Kramers–Kronig dispersion relations and the same relations hold for Δn and Δk as discussed below.

In Silicon the linear electro-optical effect is zero due to crystal symmetry while it has been known that the optical absorption spectrum of silicon is modified by external electric fields (the Franz–Keldysh effect) or by changes in the material's charge-carrier density. Starting with an experimental knowledge of the modified spectrum $\Delta\alpha(\omega, E)$ or $\Delta\alpha(\omega, \Delta N)$, *Soref* and *Bennett* have computed [5] the change in the index Δn.

The Kramers–Kronig coupling between Δn and $\Delta\alpha$ has been specified in several textbooks and journal articles, as follows:

$$\Delta n(\omega) = \frac{c}{\pi} P \int \frac{\Delta\alpha(\omega')\mathrm{d}\omega'}{\omega'^2 - \omega^2}, \tag{1}$$

where P denotes the principal value of the integral. By injecting free carriers, absorption may be modified:

$$\Delta\alpha(\omega, \Delta N) = \alpha(\omega, \Delta N) - \alpha(\omega, 0) \tag{2}$$

or α may be changed by an applied electric field:

$$\Delta\alpha(\omega, E) = \alpha(\omega, E) - \alpha(\omega, 0) \tag{3}$$

2.1.1 Electric Field Effects

The Franz–Keldysh effect, which alters the α spectrum of c-Si, is field-induced tunneling between valence and conduction band states. In recent years, the generic term electroabsorption has been adopted for $\Delta\alpha$ versus E effects.

The electroabsorption spectrum at the indirect edge has been measured in detail by *Wendland* and *Chester* [6]. Their experimental data are given in Fig. 1.

Soref and *Bennett* [5] have performed numerical caluclation to investigate electrorefraction end the results are reported in Fig. 2. Δn was then expressed as a function of optical wavelength from 1.00 to 1.60 µm. It is found that Δn is positive for $\lambda > 1.05$ µm, and that Δn is a strong function of wavelength. Starting at 1.3 µm, as λ is decreased towards the gap wavelength, Δn rises rapidly and reaches a maximum at 1.07 µm, a wavelength slightly below the nominal λ_g. Then, as λ decreases further, Δn decreases and becomes negative. They find at 1.07 µm that $\Delta n = 1.3 \times 10^{-5}$ for and external field of 100 kV/cm.

The change in index as a function of applied E field is plotted in Fig. 3 at the optimum 1.07 µm wavelength and at the nearby 1.09 µm wavelength.

Another "pure field effect", the Kerr effect, is present in Si. *Soref* [5] has estimated the strength of the Kerr effect in c-Si using the anharmonic oscillator model of *Moss* [7]:

$$\Delta n = -3e^2(n^2 - 1)\frac{E^2}{2nM^2\omega_0^4 x^2} \tag{4}$$

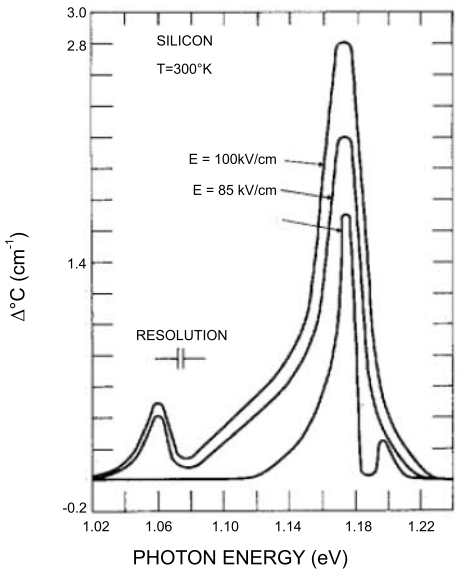

Fig. 1. Experimental electroabsorption spectrum of c-Si after *Wendland* and *Chester* [6]

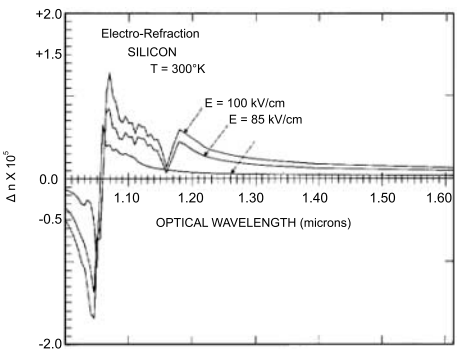

Fig. 2. Electrorefraction spectrum of c-Si [5]

here, e is the electronic charge, n is the unperturbed refractive index, M is the effective mass, ω_0 is the oscillator resonance frequency, and x is the average oscillator displacement.

2.1.2 Charge-Carrier Effect

The optical properties of silicon are strongly affected by injection of charge carriers into an undoped sample (ΔN) or by the removal of free carriers from a doped sample ($-\Delta N$). Optically, it does not make much difference whether carriers come from impurity ionization or from injection. Thus, an equivalence is assumed here.

Three carrier effects are important: 1. traditional free-carrier absorption, 2. Burstein–Moss bandfilling that shifts the α spectrum to shorter wavelengths, and 3. Coulombic interaction of carriers with impurities, an effect

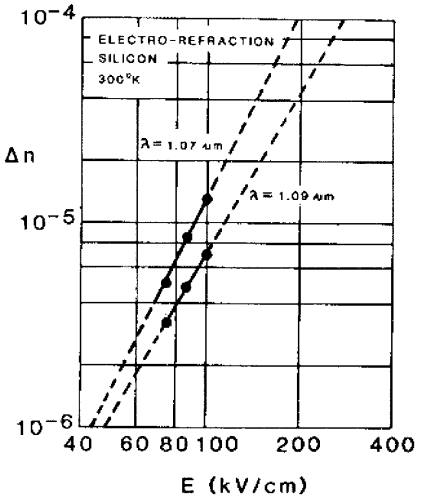

Fig. 3. Field dependence of electrorefraction [5]

that shifts the spectrum to longer wavelengths. These act simultaneously. What is experimentally observed is a redshift; thus, Coulombic effects are stronger than bandfilling in c-Si (see [8] and [9]).

For impurity concentrations in the $1 \times 10^{18}\,\mathrm{cm}^{-3}$ to $1 \times 10^{20}\,\mathrm{cm}^{-3}$ range, Schmid [8] has given detailed absorption spectra for n-type and p-type silicon in both the transparent ($h\nu < E_g$) and opaque ($h\nu > E_g$) regions covering $0.6\,\mathrm{eV} < h\nu < 1.5\,\mathrm{eV}$. Spitzer and Fan [10] also present data for n-type material over a wide infrared range from 0.025 eV to 1.1 eV. They find a weak absorption band from 0.25 eV to 0.82 eV.

Using the above data, Fig. 4 and Fig. 5 are a composite drawing of optical absorption versus $h\nu$ for various concentrations ΔN of free electrons and holes. For the undoped material in Fig. 4, the data of *Dash* and *Newman* [11], *Spitzer* and *Fan* [10], and *Schmid* [8] has been used. Over the 0.25 eV to 0.82 eV range, *Schmid*'s doping curves have been extrapolated to follow the spectral shape of *Spitzer* and *Fan*'s data.

In n-type Si, for wavelengths longer than the 5 μm absorption band edge, the experimental results of [10] show that free-carrier absorption follows a λ^2 law out to $\lambda = 50\,\mu\mathrm{m}$ for samples with $8 \times 10^{16}\,\mathrm{cm}^{-3}$ doping. In addition, *Balkanski* and *Besson* [12] observe that a in n-type samples saturates or "levels off" over the 50 μm to 87 μm range. *Randal* and *Rawcliffe* [13] find that the $\alpha(\lambda)$ spectrum is flat from $\lambda = 100$ to 500 μm. For these reasons, Fig. 4 curves should include a leveling off of α in the far infrared, as well as the α-λ^2 middle-infrared behavior mentioned above.

Schumann et al. [14] have presented a curve of α versus ΔN in n-type Si at the 87 μm wavelength, a curve reproduced here as Fig. 6.

On this curve, the experimental result of [12] have been reported. Also plotted in Fig. 6 is a theoretical curve for p-type Si, a curve drawn through

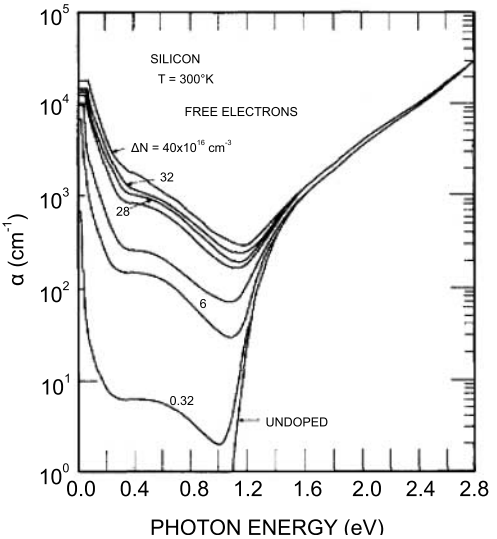

Fig. 4. Free electrons density dependence of absorption as a function of the photon energy after *Soref* and *Bennett*

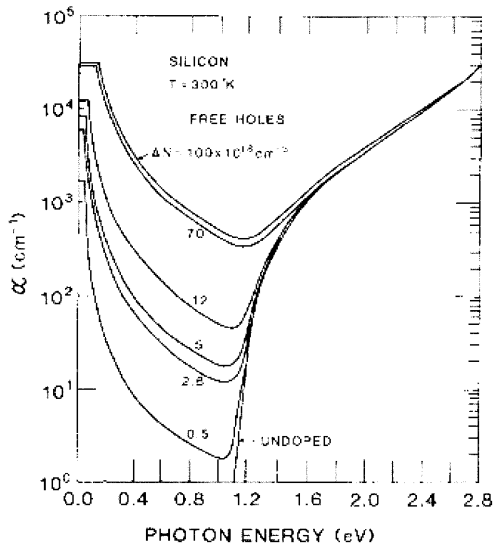

Fig. 5. Free holes density dependence of absorption as a function of the photon energy after *Soref* and *Bennett*

the two experimental data points of *Walles* and *Boija* [15,16]. The saturation of α at low frequencies is also consistent with the reflectivity measurements of *Schumann* and *Phillips* [17]. Above each plateau, an ω^{-2} extrapolation is used in Fig. 4. In the higher frequency portion of Fig. 4, ($h\nu > 1.2\,\mathrm{eV}$), the various curves are assumed to merge smoothly into the undoped curve as shown. The merger is complete above 2.8 eV. In Fig. 4, the range of integration used for the Kramers–Kronig inversion was 0.001 eV to 2.8 eV.

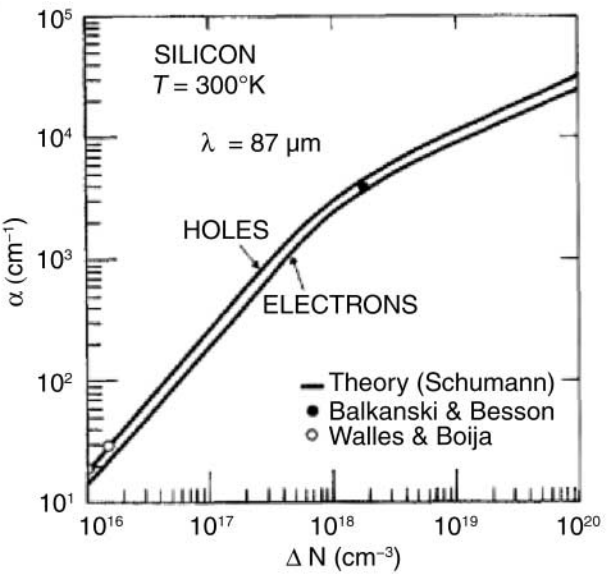

Fig. 6. Field dependenca of electrorefraction after *Soref* and *Bennett*

2.1.3 Drude's Model

The most used way to predict the change in refractive index and absorbtion coefficient is a simple free-carrier or Drude model of c-Si. The well-known formulas for refraction and absorption due to free electrons and free holes are as follows:

$$\Delta n = -\frac{e^2\lambda^2}{8\pi^2 c^2 \epsilon_0 n} \times \left(\frac{\Delta N_\mathrm{e}}{m^*_\mathrm{ce}} + \frac{\Delta N_\mathrm{h}}{m^*_\mathrm{ch}} \right) \tag{5a}$$

$$\Delta \alpha = \frac{e^3\lambda^2}{4\pi^2 c^3 \epsilon_0 n} \times \left(\frac{\Delta N_\mathrm{e}}{m^*_\mathrm{ce}\mu_e} + \frac{\Delta N_\mathrm{h}}{m^*_\mathrm{ch}\mu_\mathrm{h}} \right) \tag{5b}$$

where e is the electronic charge, ϵ_0 is the permittivity of free space, n is the refractive index of unperturbed c-Si, m^*_ce is the conductivity effective mass of electrons, m^*_ch is the conductivity effective mass of holes, μ_e is the electron mobility, and μ_h is the hole mobility. An empirical expression for both Δn and $\Delta \alpha$ evaluation at $\lambda = 1.55\,\mu\mathrm{m}$ has been reported by *Soref* and *Lorenzo* in [33] ans is recalled in the followng equations:

$$\Delta n = \Delta n_e + \Delta n_h = -\left[8.8 \times 10^{-22} \times \Delta N_\mathrm{e} + 8.5 \times 10^{-18} \times (\Delta N_\mathrm{h})^{0.8}\right] \tag{6a}$$

$$\Delta \alpha = \Delta \alpha_e + \Delta \alpha_h = 8.5 \times 10^{-18} \times \Delta N_\mathrm{e} + 6.0 \times 10^{-18} \times \Delta N_\mathrm{h}\,. \tag{6b}$$

2.2 Thermo-optic Effect in Crystalline Silicon

The refractive index of the optical materials is not a constant parameter over the temperature range in which the materials, such as crystals, semiconductors, and glasses are used in different optical devices or systems. The variation of the refractive index with the temperature at a constant pressure is called the thermo-optic coefficient. It is denoted as $\mathrm{d}n/\mathrm{d}T$, where n and T are the refractive index and the temperature, respectively. Its unit is per degree centigrade or Kelvin. Normally, the value of $\mathrm{d}n/\mathrm{d}T$ is very small, of the order of $10^{-3}\,\mathrm{K}^{-1}$ to $10^{-6}\,\mathrm{K}^{-1}$. Although the value is quite small, this phenomenon can determine the incorrect functioning of devices where the wavelength dependence scales with the refractive index, like distributed feedback lasers, couplers, interferometers, and waveguides. It can be also exploited for the design of thermally activated devices, like switches, modulators, tunable lasers, wavelength demultiplexers, and filters.

The increasing attention to the optoelectronic use of silicon has clearly solicited further optical characterization efforts. Among the optical properties of this material, the temperature dependence of the absorption and the refractive index have obviously received wide attention, both in crystalline and amorphous silicon, at photon energies around and below the energy gap.

The direct extraction of $\mathrm{d}n/\mathrm{d}T$ from the measurement of the refractive index usually poses problems arising from the weakness of the effect. For this reason, some standard techniques, which may seem simple in principle, like those requiring the use of prism-shaped specimens, are often ineffective, or require in fact complicated experimental setups to give reliable results. Recently proposed techniques, on the other hand, allowing the indirect determination of the thermo-optic coefficient from the analysis of the temperature-dependent operation of diffraction-grating-based photonic devices, present the drawback of the ad hoc realization of complex integrated test structures.

Lautenschlager et al., for instance, have measured the complex dielectric function of Si [18] in the energy range 1.7 eV to 5.7 eV, and from 20 K to 850 K, by using an ellipsometric technique. In [19] the optical absorption for both crystalline and amorphous silicon was measured at $\lambda = 1.06\,\mu\mathrm{m}$ from room temperature to about 350 °C. Recommended values of n measured by many authors at various wavelengths and temperatures were collected in [20]. A simple linear dependence of n from T in the range between 25 °C and 750 °C was reported in [21] for crystalline silicon at photon energies above 0.8 eV. *Bertolotti* et al. [22] reported on the measurement of the refractive index in several semiconductors, including silicon, for $\lambda = 0.8\,\mu\mathrm{m}$ to $12\,\mu\mathrm{m}$. Unfortunately, these data were taken in the limited temperature range between 15 °C and 35 °C. A first physically meaningful model of $n(\lambda, T)$, whose validity extends to deep infrared radiation, was proposed in [23]. Indirect measurements of crystalline silicon thermo-optic coefficient at $\lambda = 1.55\,\mu\mathrm{m}$, and at room temperature, are reported in [24], returning a value of $2.0 \times 10^{-4}\,\mathrm{K}^{-1}$.

It is obvious that for more than twenty years researches are carried out for measuring thermo-optic coefficient, but only in recent times it is possible to find in literature direct characterization of the thermo-optic effect at typical telecommunication wavelengths of 1.3 μm and 1.55 μm, and theoretical models useful to explain it. In fact, a simple technique exists, based on the multiple-beam interference principle, which has demonstrated to give reliable results [25]. This technique is direct, and is based on the measurement of temperature variation necessary to cause a complete optical detuning in a Fabry–Perot filter. In its simplest form, this test structure is a one dimensional device, actually an etalon obtained by optical polishing on both sides of a chip made of the material under testing. A first direct measurement of this important parameter, based on this method, was carried out in [25]. The interferometric technique permitted also taking into account the etalon thermal expansion, producing a more accurate evaluation $\mathrm{d}n/\mathrm{d}T = (1.86 \pm 0.08) \times 10^{-4}\,\mathrm{K}^{-1}$. The authors note that thermal expansion effect contributes very little to the étalon detuning. In fact, the ratio between the phase changes induce by thermo-optic effect and by thermal expansion is about 20. In [26] authors intend to contribute to the available data pool with a large set of direct measurements of the thermo-optic coefficient $\mathrm{d}n/\mathrm{d}T$ in crystalline silicon from 300 K to 550 K. The reported values have been obtained at $\lambda = 1.55$ μm, one of the important wavelengths in fiber-optic communication applications.

Measurements in [26] were carried out on c-Si samples with different crystal plane orientations and thicknesses. In particular, the samples were taken from several (111), (100), or (110) wafers, with resistivities in the range of $10\,\Omega \cdot \mathrm{cm}$ to $100\,\Omega \cdot \mathrm{cm}$, indifferently p- or n-type. The wafers were previously lapped for thinning and then polished on both sides to an optical degree with a colloidal silica polishing suspension. The uncertainty in the measurement of the sample thickness was 3 μm. The values of $\mathrm{d}n/\mathrm{d}T$ are reported in Fig. 7 from room temperature to 550 K, distinguished for sample type.

The authors estimate that the plotted data can be affected by an 8% error due to uncertainties in the sample thickness, experimental setup alignment procedure, and in the actual sample temperature at each measurement step. It is worthwhile noting that, given this experimental error, no difference seems to hold for $\mathrm{d}n/\mathrm{d}T$ among the considered sample types. Moreover, in [26] it is also provided a polynomial interpolation of experimental data, which gives a weak quadratic dependence of $\mathrm{d}n/\mathrm{d}T$ from T expressed in kelvin:

$$\frac{\mathrm{d}n}{\mathrm{d}T} = 9.48 \times 10^{-5} + 3.47 \times 10^{-7} \times T - 1.49 \times 10^{-10} \times T^2 \quad \left(\mathrm{K}^{-1}\right) \qquad (7)$$

A recent and comprehensive theoretical paper on physical modeling of thermo-optic effect is [27], where the analysis of the temperature dependence of the thermo-optic effect in silicon is reported, and the results obtained are compared with experimental data. The analysis is carried out in the technologically exploitable temperature range 300 K to 600 K, and centered at

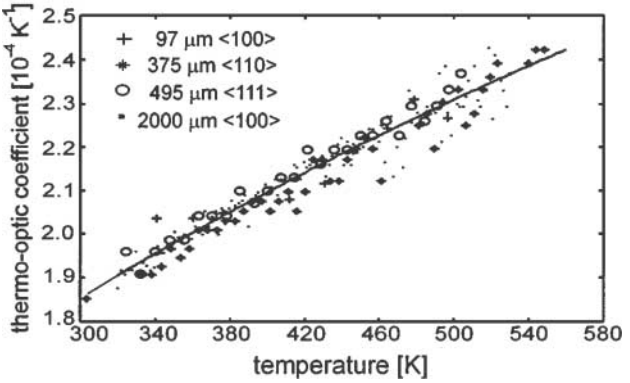

Fig. 7. Measured thermo-optic coefficient in various silicon samples. Interpolation of data as a second-order polynomial is shown as a *solid line* [25]

the principal optical communication wavelength of 1.55 μm. In particular, single and double oscillator approximations, previously proposed to model the refractive index and the thermo-optic coefficient frequency dispersions, have been extended to explain its temperature dependence in the cited temperature range. The reported approach highlights the role of the parameters determining the temperature dependence of the interband transition energies at the critical points of the combined density of states, whose values are also estimated by best fitting procedures. Such values are in good agreement with those reported in other works.

Using a single oscillator approximation, authors obtain:

$$\frac{\mathrm{d}n}{\mathrm{d}T} = \frac{n^2 - 1}{2n}\left[-3k_{\mathrm{ex}} - \frac{2}{E_g}\frac{\mathrm{d}E_g}{\mathrm{d}T}\frac{1}{1-(E/E_g)^2}\right] \tag{8}$$

where n and k_{ex} are both dependent on the temperature. Experimental data (in Fig. 8) are fitted by means of (8), expressing $\mathrm{d}E_g/\mathrm{d}T$ as the sum of two terms, at constant volume and at constant temperature respectively:

$$\frac{\mathrm{d}E_g}{\mathrm{d}T} = \left(\frac{\partial E_g}{\partial T}\right)_V + 3k_{\mathrm{ex}}V\left(\frac{\partial E_g}{\partial V}\right)_T \tag{9}$$

where, for semiconductors, the partial derivative with respect to the volume can be neglected.

Concerning the band-gap temperature dependence, we adopt the simple and widely quoted empirical relation given by:

$$E_g(T) = E_g(0) - \frac{\alpha_g T^2}{(T+\beta_g)} \tag{10}$$

where $E_g(0)$ is the average band-gap energy at 0 K, the constant α_g is related to the electron–phonon interaction, and β_g is related to the Debye temperature of the semiconductor. The thermal expansion coefficient k_{ex} of silicon is

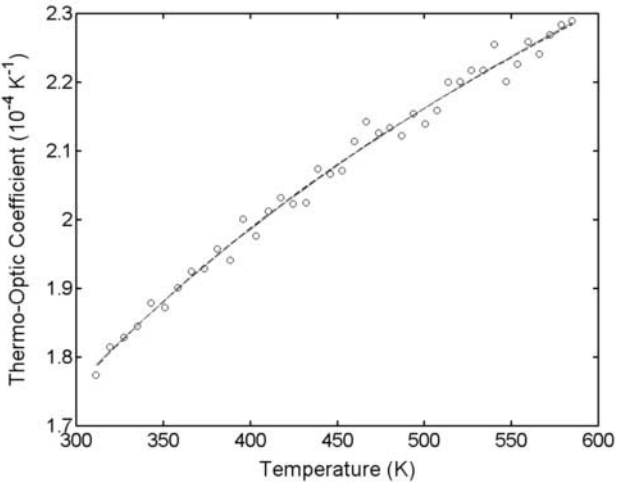

Fig. 8. Experimental results of the thermo-optic coefficient in silicon, and best-fit curves obtained with single (*dashed line*) and double (*solid line*) oscillator approximations. [26]

a well known parameter. The single oscillator fitting procedure involves the three floating parameters $E_g(0)$, α_g and β_g (see (8), (9), and (10)). Table 1 summarizes the parameter values resulting from the fitting procedure with the corresponding uncertainties. In the same paper [27] is discussed another theoretical model based on a semi empirical method for the calculation of the refractive index of semiconductors with diamond and zinc-blende structures at photon energies smaller than the band-gap energy [28]. Using this approach the authors have demonstrated that the thermo-optic coefficient of an indirect gap semiconductor can be written as a function of two elementary oscillators and, once again, it is possible to fit experimental data with a function of six floating parameters. In Fig. 8 the resulting best fitting curve is reported, which is not so different from the single oscillator model curve. The discussion of this model is beyond our purpose, and for that reason we refer to [27].

Table 1. Parameters involved in the single oscillator fitting procedure. The 95% confidence limit is given in parentheses

Single Oscillator	$E_g(0)$ (eV)	α_g ($1 \times 10^{-4}\,\mathrm{eV \cdot K^{-1}}$)	β_g (K)
	4.03 (0.02)	3.41 (0.03)	439 (13)

3 Optical Schemes for the Modulation of Light

A modulator is a device with one input port and one output port, contrasted with the N optical inputs and M optical outputs of a switch. As light travels through the modulator, or is reflected off it, the optical amplitude and phase change in response to the electrical information signal. Modulation requires an active effect that modifies the complex refractive index of silicon by an amount $\Delta n + \mathrm{i}\Delta k$, where Δn is the real index shift and Δk is the change in optical extinction coefficient. Typically, these changes are induced by plasma dispersion effect or thermo-optic effect as it has been discussed in detail in the previous sections. It is obvious that a modulator is characterized by the so called chirp factor $\Delta n/\Delta k$, which indicates the efficiency of the phase modulation compared to the pure amplitude modulation. The chirp factor for plasma dispersion effect in silicon decreases when the wavelength increases. With the exception of early works, where the authors have demonstrated the feasibility of bulk devices [29], in the last years researches were carried out exclusively on active components integrated in optical waveguides. Experimentally, three basic types of silicon host waveguides were utilized: lightly doped silicon on heavily doped silicon, silicon on insulator (SOI) and epitaxial $Si_{1-x}Ge_x$ on Si. We will present devices which are realized or proposed in the first two types of waveguide, excluding the last, because it is not a pure silicon-based technology. Together with the host waveguide classification, it can be useful to distinguish the modulator on the basis of the modulation behavior, that is if they mainly modify the phase or the amplitude of the optical signal, or, in other words, if the chirp factor is much higher than 1 or about equal to 1.

3.1 Free-Carrier Absorption Based Modulators

In this paragraph we address to the operating principle of silicon optoelectronic modulators based on the pure absorption induced by Plasma Dispersion Effect, that is devices where the chirp factor is about 1. This effect has been treated in the beginning of the chapter, where we have reported the losses variation vs. plasma density relation:

$$\Delta\alpha = \frac{e^3\lambda^2}{4\pi^2 c^3 \epsilon_0 n} \times \left(\frac{\Delta N_\mathrm{e}}{m^*_\mathrm{ce}\mu_\mathrm{e}} + \frac{\Delta N_\mathrm{h}}{m^*_\mathrm{ch}\mu_\mathrm{h}}\right) \tag{11}$$

where α is the absorption coefficient and $\Delta N_{\mathrm{e,h}}$ is the variation of free carrier density.

For an integrated optoelectronic device, there are two ways to induce a variation of free carrier concentration into the active volume of the waveguide modulator, in order to modify the optical absorption of it: the injection in an undoped layer or the depletion from a highly doped one. The electronic device that can be integrated into the waveguide can be a p–i–n diode or a three terminal active device (either unipolar or bipolar).

The active electrical devices can be integrated in a low-loss Silicon-On-Insulator (SOI) waveguide (typically for p–i–n diode), or in a Silicon-On-Silicon waveguide (for the three terminal device). In what follows we will also discuss about different approaches in the electrical driving schemes.

In the late eighties, research groups have explored silicon as a material for optical interconnects [30]. All-silicon waveguides, for hosting the active device, were realized and characterized, but only recently these structures have reached performances useful for practical applications. In fact, in standard all-silicon waveguide, the high doping difference between n^{++} substrate and guiding layer causes the refractive index difference, which ensures vertical confinement for the infrared radiation propagating into the film. The lateral confinement can be provided by the etching of the top layer, so realizing the so-called *ridge* waveguide. The propagation losses for these first waveguides were in the range of 10 dB/cm to 15 dB/cm. An optimized version of the standard ridge waveguide can be designed [31] to show a single-mode operation, supporting only the first order modes for each polarization. The propagation losses of such a structure can be further reduced implanting a lower highly-doped cladding, reaching a value of about 1.2 dB/cm [32]. The second approach for the fabrication of silicon-based waveguides is characterized by very low optical losses (< 0.2 dB/cm), due to the good vertical confinement ensured by the presence of the non-absorbing SiO_2 bottom layer.

Pioneering papers in silicon optoelectronics were published by *Soref* et al. [5, 3, 33]. In these papers the authors have described the actual possibilities for silicon in the waveguiding and control of infrared optical radiation. After these preliminary proposals, several different solutions were reported in literature. Among the early works, it is useful to cite the paper by *Lorenzo* et al. [34], where a first practical application of the plasma dispersion effect is reported. In this proposal, an all-silicon waveguide hosts a X-switch, driven by a vertical p–i–n diode, working at current density of 1.26 kA/cm^2 and producing a contrast of about 3 dB. Of course, it is unrealistic to expect this unoptimized multimode device to have acceptable performances. The importance of such initial proposal, even if the subject is not a modulator in strictly sense, is in the novelty it suggests, explicitly affirming that the silicon, together with its microelectronic technology, can be used to transmit and manipulate optical signals.

In 1991 *Treyz* et al. [35] have proposed a simple absorption modulator based on the integration of a vertical p–i–n diode in an all-silicon waveguide. The performances of this device are strongly limited by the high propagation losses of the waveguide (> 20 dB/cm). The achieved modulation depth is 76% (-6.2 dB) for a driving current density of 3 kA/cm^2. Switching time is about 50 ns. In Fig. 9 is reported the transverse cross section of the modulator active region.

A similar proposal was published in 1994 by *Leistiko* et al. [36]. The modulator, realized by means of standard microelectronic techniques, showed high

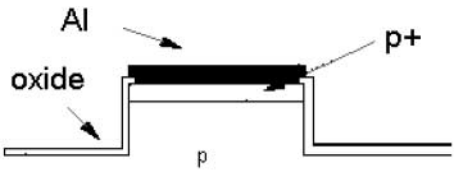

Fig. 9. Schematic diagram of the cross section of the active region for the modulator proposed in [35]

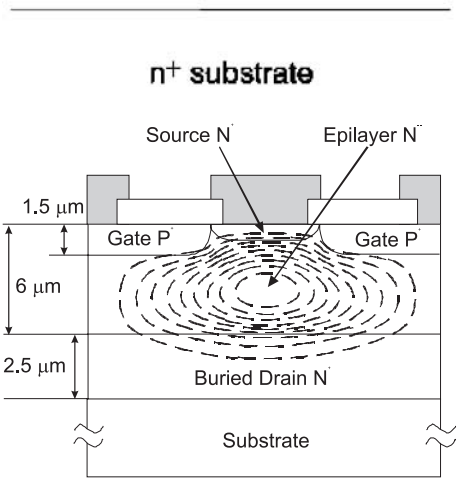

Fig. 10. Cross section of a BMFET optical modulator device

insertion losses, in the range 10 dB to 15 dB, on a total length of about 9 mm. The integrated p–i–n was formed by the n^{++} heavily doped substrate and two p^{+} diffused regions, forming also the optical channel. The measured modulation depth was nearly 100% (−30 dB) and the characteristic turn-on and turn-off time constant are approximately 20 μs.

A more efficient solution was proposed by *Cutolo* et al. [37]. A three terminal device is used to reach a high value of modulation depth with low power consumption, by exploiting phase shift and concurrent increasing optical absorption. Another advantage of such configuration is the lower value for the switching time constants. The cross section of the structure is sketched in Fig. 10.

This structure is capable, at the same time, to generate a complex refractive index variation, in order to modulate the infrared beam, and guarantee a good confinement of the optical radiation. The modulator can be considered as a 2-D optical channel waveguide, although not optimized for this purpose. From the electrical point of view, this device, to be a modulator, should be able to produce an electron–hole plasma into the central waveguiding region. Both surface highly doped regions, together with the n^{++} buried layer, carry out this function. The described structure is the elementary cell of a bipolar mode field effect transistor (BMFET). The two lateral p-type regions act as

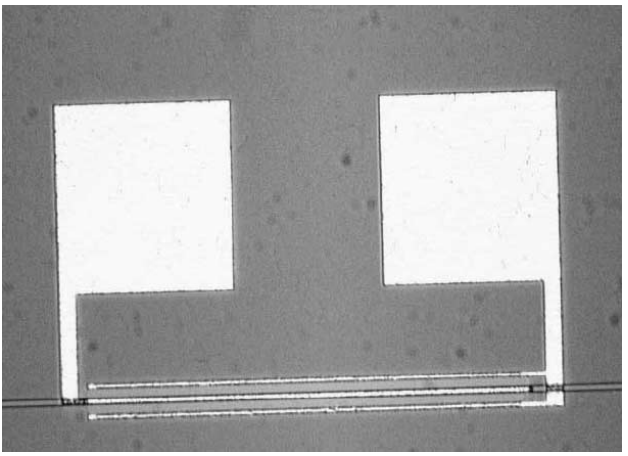

Fig. 11. Top view of a 500 μm long BMFET modulator

the gate, the central n-type region as the source, and the n^{++} buried layer plays the role of the drain.

In this kind of modulator the variation in the charge density, and consequently in the refractive index, can be much larger than carrier density resulting from injection of single polarity, like occurs in a standard FET. Moreover this structure, characterized by the presence of a control terminal connected to the n^{++} buried layer, is preferred to the simple p–i–n diode because of the use of the third electrode which allows a more accurate spatial control of the injected plasma and higher switching frequencies, thanks to the possibility to quickly control the plasma distribution into the channel by using an appropriate bias, as will be described afterwards. The predicted performances are, for a 1000 μm long amplitude modulator, M = 20% (limited to a useful value, even if in principle it is possible to reach 100%), switching power of 27.8 mW, and a switching time of about 5.6 ns.

The top view of a realized BMFET modulator is reported in Fig.11.

It is important to notice that the integration of a three terminal active device in a silicon-based waveguide force the usage of an all-silicon host structure, because of the need to realize a buried junction to control the optical characteristics of the channel, despite the higher propagating losses than a SOI waveguide. Moreover, an all-silicon waveguide is very cheap and easy to make, if compared to a SOI structure, and its thermal conductivity is very high. This fact allows a safe operation, because permits to better dissipate the heat generated during the operation, and reduces also the undesired refractive index variation produced by thermo-optic effect. In addiction, the homogeneous transverse cross section of an all-silicon modulator ensures an uniform temperature distribution in it, so avoiding undesired spatial refractive index variations, and consequently optical mode distortion, due to localized heating.

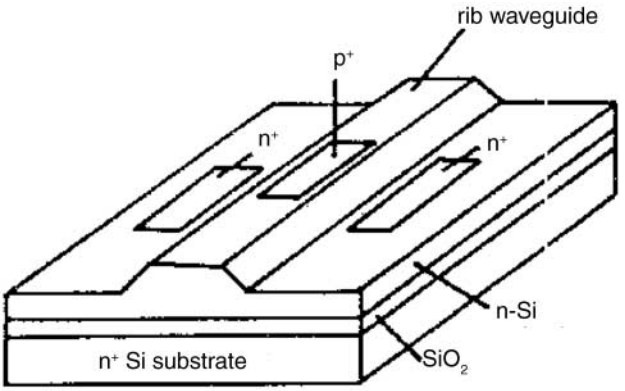

Fig. 12. Schematic of the modulator proposed in [39]

Preliminary experimental measurements carried out on this class of modulator are reported in [38], where authors show that a modulation depth of 75% can be achieved by injecting a constant hole current in the channel region from the gate ($I_G = 10$ mA), thus generating a plasma of carriers, and biasing drain-source junction from 0 V to 16 V.

With the intention to reduce the propagation losses, *Zhao* et al. [39] proposed and realized the integration of a lateral p–i–n diode into a SOI ridge waveguide (see Fig. 12).

The modulator operation is based on the waveguide-vanishing effect, induced by free carrier injection together with usual free carrier absorption. The total insertion losses of the device are measured to be 3.65 dB, the modulation depth is 96% at an injection current of 45 mA. Response time is about 160 ns. The waveguide-vanishing effect is induced by the reduction of the refractive index in the waveguide core. This causes a lot of guided-mode energy to be lost and absorbed in the ridge waveguide, which will cause the guide itself to cut-off. Consequently, there is a concurrent effect of the plasma induces absorption and refraction.

3.1.1 Electrical Driving Schemes

Almost all the modulators presented so far rely on the electrical mechanism of free carriers injection using a p–i–n diode. This two-terminal device, from the electrical point of view, acts as a diffusion capacitor which has to be filled with carriers through a suitable current source.

On the other hand, when dealing with three terminal devices some discussion can be made about the optimal driving scheme to be exploited in order to guaranteed that good optical switching is not limited by slow electrical mechanisms. In order to shed some light on the latter assumption we refer to the paper of *Cutolo* et al. [37] where a three-terminal optical modulator has been analyzed in detail with respect to the electrical driving conditions.

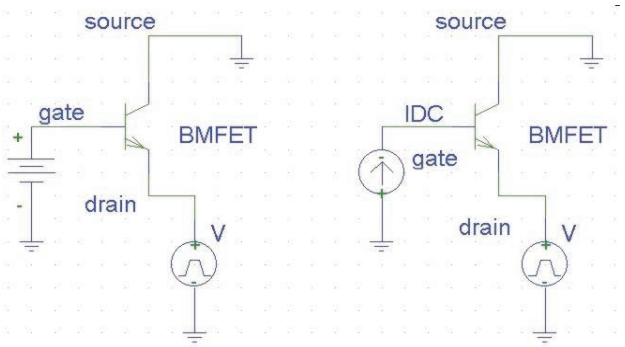

Fig. 13. Electrical driving circuit to switch optical BMFET device

They compare how it is possible to use a three terminal device as a p–i–n diode simply switching the current on and off on the GATE terminal. This way, though easy, results in very low switching characteristics because the epilayer has to be filled and depleted and little can be done about the storage of electrons and holes inside the epilayer after the removal of the GATE current [2,37].

From steady-state simulations performed on a 1000-μm-long device, *Cutolo* et al. [37] have evaluated that, in order to reach the desired modulation depth, the epilayer must be filled with a concentration of electrons and holes of $5 \times 10^{16}\,\mathrm{cm}^{-3}$. This, on its turn, is obtained by biasing the GATE terminal with a $0.1\,\mathrm{mA}/\mu\mathrm{m}$ current. This information can be exploited in different ways in order to switch the optical signal off.

One possiblity to obtain faster performances is by fixing the DRAIN bias with a positive voltage source and then switching the gate control current on and off. They also presented the so-called *Plasma-Drift* driving scheme which has been also used by *Sciuto* et al. [38] to obtain their preliminary experimental results.

These are only two of the possible driving schemes and the first is the one which mostly resembles the switching of a bipolar transistor. In the *Plasma-Drift* configuration, the driving voltage is applied simultaneously to the GATE and to the DRAIN terminal (see Fig. 13). By doing so total charge present in the epilayer is fixed by the GATE current to the amount required to have the required modulation depth while the positive voltage pulse applied to the DRAIN depletes the central region of the waveguide. This results in a faster switching speed since it is not necessary to deplete the epilayer but it is just needed to remove the positive voltage from the DRAIN allowing the electron–hole plasma to redistribute uniformly across the optical channel. In addition to that the recombination process do no affect the switching speed in a relevant way.

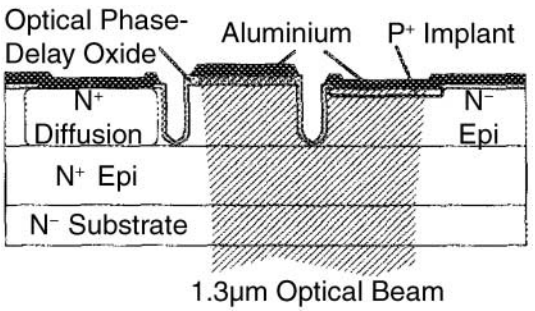

Fig. 14. Schematic cross section of the modulator proposed by *Hemenway* et al. [40]

3.2 Interferometric Structures for Optical Modulation in Silicon

In this paragraph we will discuss on pure phase modulators, ($\Delta n/\Delta k \gg 1$), and modulators where the phase modulation is converted in amplitude modulation using an interferometric optical structure, external or internal to the modulator itself, working in the II and III window for fiber optic communications ($\lambda = 1.3\,\mu m$ and $1.55\,\mu m$). The physical effects exploited for the generation of a phase change are typically the plasma dispersion effect and the thermo-optic effect, discussed in a previous paragraph. Starting from early proposals, several authors have published papers on pure phase modulators for infrared light beam. The compatibility with microelectronic technologies is another attractive characteristic common to most of the proposed or realized devices.

3.2.1 All-Silicon Modulators

The first proposals of phase modulator integrated in all-silicon waveguides are contemporaneous to the early amplitude modulators we discussed in the previous paragraph. *Hemenway* et al. [40] in 1989 have reported an all-silicon reflection-type optical amplitude modulator, which uses free-carrier dispersion effect to spatially modulate the phase of an optical beam. Subsequent phase-modulation to amplitude-modulation conversion occurs by mode selection in the coupled single-mode fiber. Inside the device (see Fig. 14) one half of the beam is phase delayed relative to the other half. The phase delay consists of two parts, a static delay of $\lambda/4$ and a separate, modulated delay due to free-carrier injection. This device allows reaching a modulation depth of about 35%, at a driving peak current is 26 mA. At low and intermediate drive levels, the frequency response is flat, showing a -3 dB bandwidth of 200 MHz.

Treyz et al. [41] proposed a more canonical interferometric configuration in 1991. Device operation is based on the plasma dispersion effect and is implemented in the Mach–Zehnder interferometer configuration. As shown

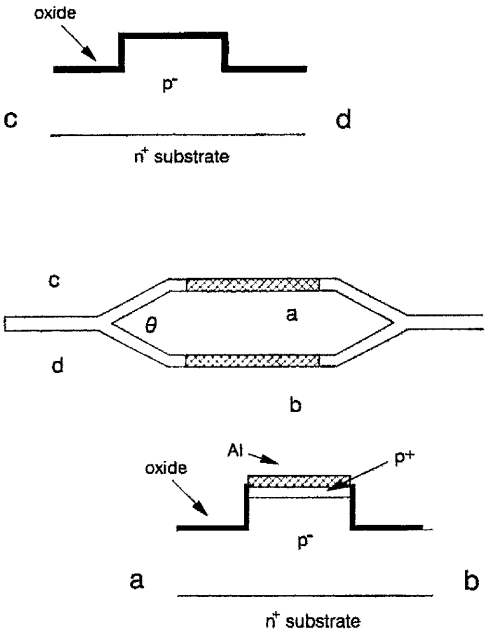

Fig. 15. Schematic diagram of the interferometer proposed by *Treyz* et al. [41]

in Fig. 15 the interferometer consists of passive all-silicon waveguide and p–i–n diode. For a current density of 1.6 kA/cm^2, the injected carrier is about 6.5×10^{17} cm^{-3}, and the achieved modulation depth is 4.9 dB. Response time of less than 50 ns has been obtained. Despite the simplicity of this modulator, its drawback is the poor quality of the passive host waveguide, whose propagation losses are greater than 20 dB/cm.

In the same year *Xiao* et al. [42] proposed a non-integrated modulator which consists essentially of a high-finesse Fabry–Perot resonant cavity formed by two silicon dioxide mirrors, and a p–i–n diode optical phase modulator placed inside the cavity. Although the novelty of the proposal, the performances are rather low; the modulation depth of 10% is achieved with a current density of 6.0 kA/cm^2. The -3 dB bandwidth is about 40 MHz. In 1994 the same research group realized an optimized version of a similar structure [43], where the carrier effect was produced by optical generation and not by an electronic device integrated in the optical structure. The 100-fs-long pulsed pump beam, with a wavelength of 850 nm, was focused into an asymmetric Fabry–Perot cavity, which is sketched in Fig. 16. The resulting real refractive index variation $\Delta n = 5.0 \times 10^{-3}$, corresponding to a generated free carriers density is about 2.0×10^{18} cm^{-3}, is converted in an amplitude modulation of 10 %, with a typical switching time of about 2 ns.

Another version of partially integrated Fabry–Perot optical modulator was proposed by *Cocorullo* et al. [44] in 1994. The device is a simple silicon chip, whose opposite transverse facets were polished in order to act as a cavity

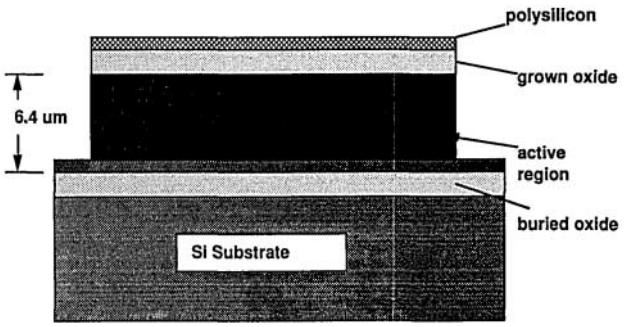

Fig. 16. Cross section of the asymmetric Si Fabry–Perot étalon proposed by *Liu* et al. [43]

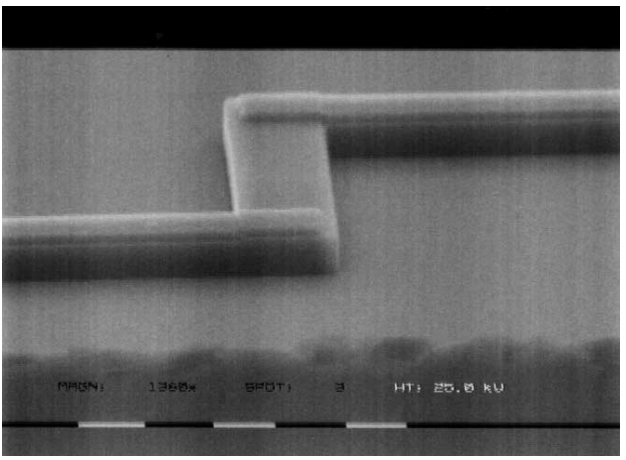

Fig. 17. SEM picture of the Si Fabry–Perot modulator realized by *Cocorullo* et al. [45]

mirrors. The structure can be considered a large slab waveguide, heated by Joule effect, thanks to the current flowing in an aluminum film deposited on the top. A thin n^+ layer under the metal heater avoids large optical field attenuation. In this way it is possible to induce a refractive index variation by thermo-optic effect. Maximum achieved modulation depth is 55% and typical switching time constants are greater of 200 µs. The above described work was preparatory for an integrated version of a similar device. In effect, the first proposal of a Fabry–Perot modulator integrated into an all-silicon optical waveguide was reported by *Cocorullo* et al. [45] in 1997. In this device, whose SEM picture is shown in Fig. 17, an unoptimized all-silicon multimode waveguide hosts a thermo-optic Fabry–Perot modulator.

The cavity mirrors are realized by wet etching and the heating element is made by a doped polysilicon film. The whole structure is fully compatible

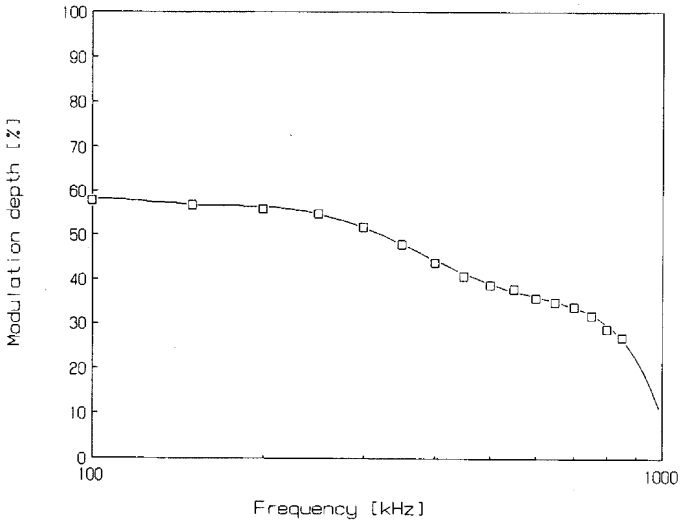

Fig. 18. Frequency response of the Si Fabry–Perot integrated modulator [45]

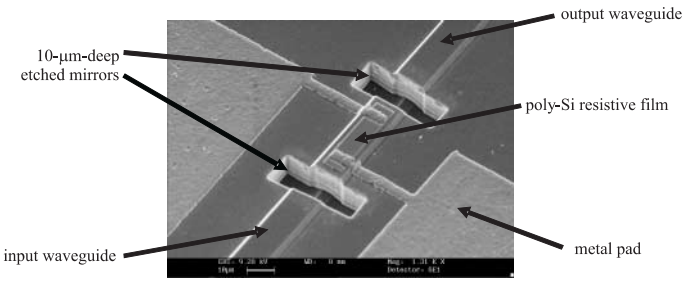

Fig. 19. SEM picture of the Si Fabry–Perot integrated modulator realized by *Iodice* et al. [46]

with microelectronic technologies. The performances are, nowadays the best reported in literature for thermo-optic silicon modulator. The modulation depth is about 60%, for a driving energy of 0.2 μJ. The −3 dB bandwidth is 700 kHz (see Fig. 18) and operation up to 1.2 MHz, with a reduced modulation depth, was observed.

A further optimization of this integrated modulator was proposed by *Iodice* et al. [46], where the device is integrated in a low-loss single-mode all-silicon waveguide (propagation losses $\simeq$ 1.0 dB/cm) and the cavity is defined by means of anisotropic reactive ion etching (see Fig. 19).

In this paper it is also discussed an optimization of the driving signal which permits to achieve a transmission rate of 2.2 Mb/s, at maximum modulation depth of 70% and energy expenses per cycle of about 0.9 μJ.

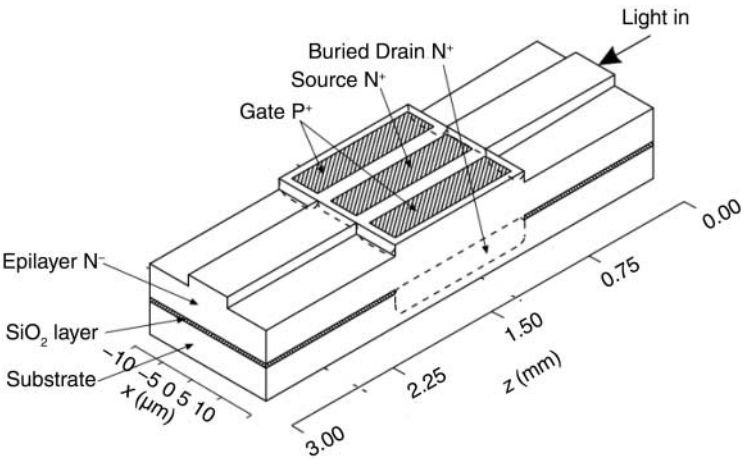

Fig. 20. BMFET optical modulator proposed by *Cutolo* et al. [37]

Beside the experimental papers above discussed, several theoretical proposals are reported in literature. Actually, in most cases these proposals are limited to numerical or analytical models with difficult or even impossible realization, but some papers suggest interesting operation principles or optical configurations. *Friedman* et al. [47] proposed and analyzed a singular integration between a new dual-injection field effect transistor in a standard all-silicon waveguide for light modulation.

For a driving source-drain voltage of 320 mV, the effective refractive index of the waveguide mode changes by $\Delta n = 1 \times 10^{-3}$ when the gate voltage is 12 V. The figure of merit $\Delta\phi/(V \times L)$ is $23°/(\mathrm{V} \cdot \mathrm{mm})$ and the chirp factor is $\Delta n/\Delta k = 16$. Switching characteristics of the gate-controlled modulator are very fast and it is governed by the sweep-out of the mobile charges.

The authors estimated a −3 dB bandwidth of about 3.2 GHz, limited by the RC time constant of the device. Another original proposal published by *Cutolo* et al. [37] describes a bipolar-mode field effect transistor integrated in a silicon waveguide acting as pure amplitude or pure phase modulator. In Fig. 20 is sketched the structure of such a device.

When driven at low injection level ($\Delta N = 2.0 \times 10^{17}\,\mathrm{cm}^{-3}$, that is with $\Delta n/\Delta k = 21.6$, the figure of merit for pure phase modulation behavior attains the record value of $215°/(\mathrm{V} \cdot \mathrm{mm})$. The operation power is also very low, about 43 mW. Accepting the price of rather high switching power, forcing the injected plasma by using the third control terminal (the so-called plasma-drift operation mode), it was calculated that the typical time constant can reach a value smaller than 3.5 ns. Realization in standard microelectronic technologies and preliminary characterization are reported in [2].

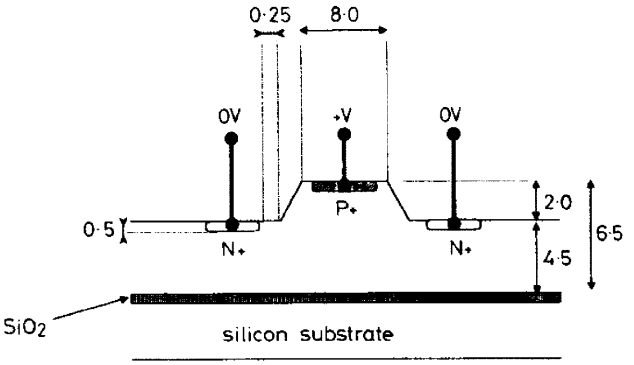

Fig. 21. Transverse cross section of the modulator realized by *Tang* et al. [49]

3.2.2 Silicon-On-Insulator Modulators

The need for a low-loss host waveguide for the integration of active devices pushed during last ten years several research groups in investigating the so-called SOI (Silicon-On-Insulator) structures. With this name is generally indicated an optical waveguide, slab or ridge, where the lower cladding is a silicon dioxide buried layer and the guiding film is in crystalline silicon. Several fabrication techniques can be exploited for realizing such structures: oxygen ions implantation (SIMOX) and bonded and etch back (BESOI) are practically useful for commercial production. The first proposals and realizations of optoelectronic modulator begun to appear in literature when commercial SOI wafers with good characteristics became available at low cost. In 1991 *Treyz* et al. [48] realized the first Mach–Zehnder modulator integrated in a SOI waveguide. The modulation mechanism was based in the thermally induced refractive index variation in the crystalline silicon guiding film. A driving power of 30 mW, dissipated in the NiCr heater realized on the top of one interferometer arm, allows reaching a modulation depth of 40% with time constant of about 50 µs. The first realization of an electrically controlled phase modulator, which integrated a lateral p–i–n diode into a SOI waveguide, was published by *Tang* et al. [49]. In Fig. 21 is reported the transverse cross section of the realized device.

The host waveguide exhibited low propagation losses ($< 1.0\,\mathrm{dB/cm}$) and the modulator, characterized in an external Mach–Zehnder interferometer, had a high figure of merit of about $200°/(\mathrm{V}\cdot\mathrm{mm})$. The electrical power needed for a complete detuning of the interferometer was about 12 mW, the injection level $\Delta N = 2.5 \times 10^{17}\,\mathrm{cm}^{-3}$, and the refractive index variation $\Delta n = 1.5 \times 10^{-3}$. This device was not characterized dynamically. An integrated version of the Mach–Zehnder interferometer in a SOI waveguide, with a lateral p–i–n diode as driving element, was published by *Zhao* et al. [50] in 1995. The structure layout and its cross section are reported in Fig. 22.

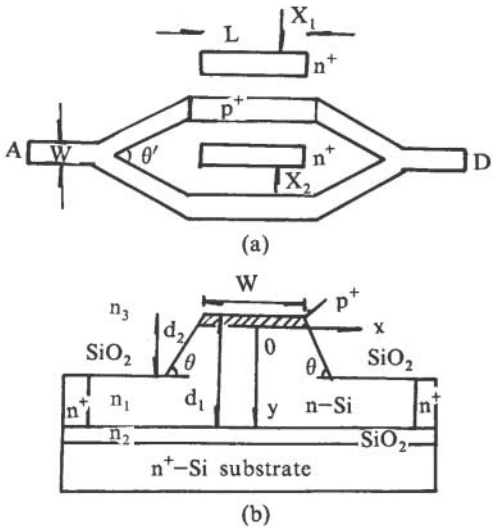

Fig. 22. Schematic structure and transverse cross section of the modulator realized by *Zhao* et al. [50]

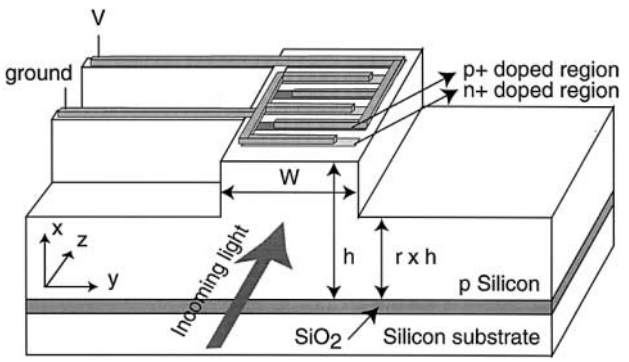

Fig. 23. Schematic view of the phase modulator realized by *Dainesi* et al. [51]

The insertion loss and modulation depth are measured to be 4.81 dB and 98%, respectively, at the wavelength of 1.3 μm when the forward bias voltage applied to the p–i–n diode is 0.95 V. The switching time constant of the device was measured to be less than 0.2 μs. To improve response speed of the modulator, electron irradiation is performed at electron energy of 14 MeV. Another CMOS-compatible fully-integrated Mach–Zehnder interferometer, realized in a SOI waveguide, and utilizing the plasma dispersion effect, was proposed by *Dainesi* et al. [51] in 2000. In this modulator a series of 66 p–i–n diodes is realized longitudinally along the top of the waveguide (see Fig. 23) at both interferometer arms.

Once again the injection level was $\Delta N = 2.5 \times 10^{17}\,\mathrm{cm}^{-3}$, which is needed to obtain a π phase shift over 1 mm long active region. A total driving current of 136 mA produces an ideal 100% modulation depth. As an injection

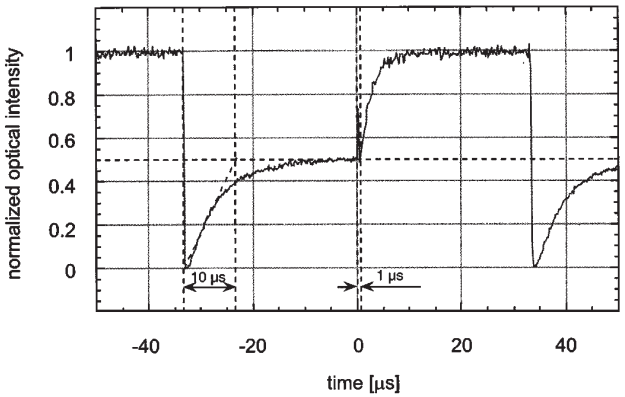

Fig. 24. Experimental optical output showing thermal and electrical phenomena [51]

of charge is always associated to power dissipation, a phase modulator based only on plasma dispersion effect is not feasible and thermo-optic effect will always be present. Because free-carrier and thermo-optic effects are opposite in sign, the resulting net modulation depth is about 50%, but the two phenomena are characterized by very different time constant and it is very easy in the time-domain output pattern to distinguish between the two effects using their respective rise times (see Fig. 24). Authors measured a bandwidth of 100 kHz for thermally induced modulation and of 10 MHz for plasma dispersion induced operation.

An abounding literature is available on theoretical proposals of SOI waveguide integrated phase modulator. Amongst the early papers, it is worthwhile to cite the proposal made by *Giguere* et al. [52]. In this paper it is depicted the integration of a MOSFET in a SOI waveguide. The plasma dispersion effect is exploited for producing an index variation of about 6.0×10^{-4}. At driving current density of 400 A/cm^2 to 800 A/cm^2, the resulting figure-of-merit is $40°/(\mathrm{V} \cdot \mathrm{mm})$. *Huang* et al. [53] in 1993 proposed a novel electronic device configuration, based on the impact ionization mechanism for carrier generation. The simulated turn-on and turn-off time was less than 1 ns, but the driving current density is greater than 100 kA/cm^2. A more conventional approach, that is a lateral p–i–n diode integrated in a rib waveguide, was followed by *Tang* et al. [54] in their paper published in 1994. The publication is particularly interesting for the accurate geometrical definition and optimization of the optoelectronic structure. The resulting figure-of-merit attains the value of $200°/(\mathrm{V} \cdot \mathrm{mm})$ for a driving current of only 10 mA. The theoretical estimated switching time is about 100 ns. A more complicated and more performing approach was proposed by *Wang* et al. [55], in a paper presenting an electrically induced Bragg reflector in a SOI waveguide. The device is sketched in Fig. 25.

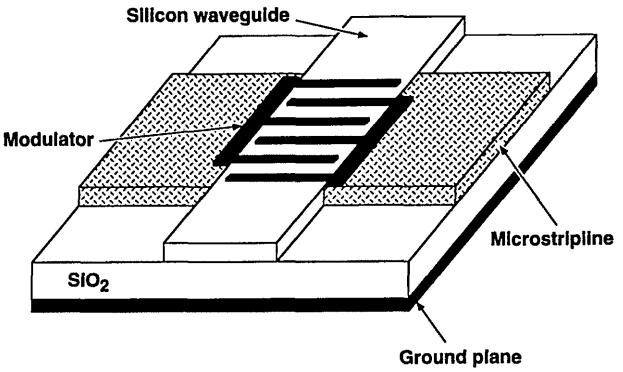

Fig. 25. Schematic view of the Bragg induced modulator proposed by *Wang* et al. [55]

The interdigitated metal fingers are alternately biased and form forward and reverse biased Schottky junctions with the heavily doped silicon film. The resulting longitudinal periodic refractive index structure, whose variation Δn is about 5.0×10^{-3}, acts as a Bragg mirror. For a 500-μm-long active region the predicted achievable modulation depth is 70%. The speed of such modulator seems to be limited by the RC time constant of the structure itself, indicating a −3 dB bandwidth in the range of 50 GHz. The main drawbacks are related to the high propagating losses of the very thin and high-doped core waveguide and to the need of electron beam lithography for defining the Bragg control structure. Further improvement of the optical structure are reported by *Liu* et al. [56], where authors discuss about a Fabry–Perot interferometer integrated in a SOI waveguide, whose mirrors are realized by means of a couple of Bragg reflectors. In this paper the realization and characterization of Bragg mirrors is presented, but the overall modulator performances are only theoretically discussed. They affirm that with an injection level $\Delta N = 10^{18}\,\mathrm{cm}^{-3}$ it is possible to completely detune the F–P cavity, reaching a 100% of modulation depth. A different approach in Bragg mirrors exploitation was suggested by *Cutolo* et al. [57]. The Bragg reflector was placed in the middle of a lateral p–i–n diode (see Fig. 26) and the amplitude modulation was achieved changing, by injection of free carriers, the Bragg resonance wavelength. Numerical simulations show a modulation depth of 50% achieved in about 12 ns with a power dissipation of 4.0 mW and an insertion loss of 1.0 dB.

Another proposal of Fabry–Perot interferometer based modulator was presented by *Vonsovici* et al. [58], where waveguide discontinuities, realized by RIE etching, play the role of the two mirrors of the interferometer. The electronic device driving the modulator is a standard lateral p–i–n diode and the reported maximum modulation depth, for a $\Delta n = 5.0 \times 10^{-4}$, is 60% at current density of $500\,\mathrm{A/cm}^2$, and with −3 dB bandwidth of about 100 MHz.

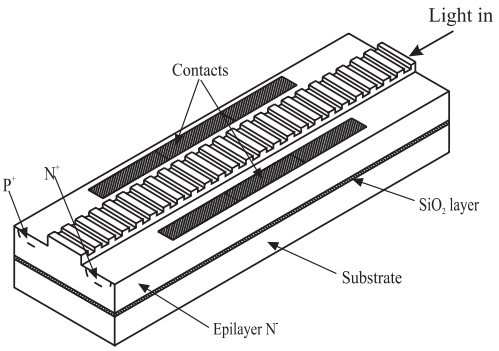

Fig. 26. Schematic view of the Bragg modulator proposed by *Cutolo* et al. [57]

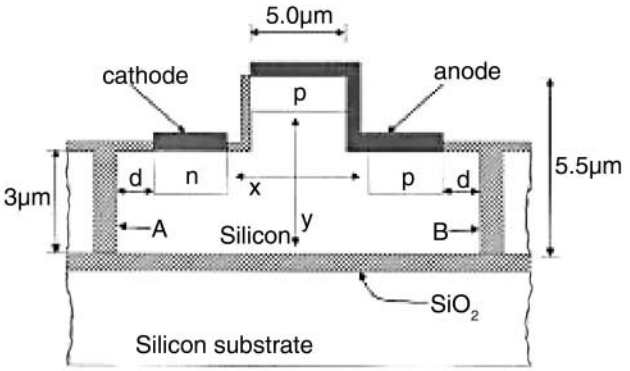

Fig. 27. Cross section of the active region of the modulator proposed by *Hewitt* et al. [61]

In the last years an optimization of the Bragg modulator presented in [57] was proposed by *Coppola* et al. [59], where are expected 4.0 ns of rise time and 0.3 mW Of Dissipated Power. A final optimization of the Bragg modulator presented in [57] has been recently presented (see [60]) where, after careful design of the host waveguide, together with the shaping of the driving signal which allows better injection/depletion of carriers, over 1.4 GHz maxiumum operation frequency has been reached.

Another solution for the enhancement of the modulation efficiency was discussed by *Hewitt* et al. [61], whose paper describes a simple p–i–n diode integrated in a SOI waveguide. The novelty of such a proposal is the presence of vertical isolation trenches laterally to the diode. The modeling indicates that increased DC and transient performances results from these trenches defined adjacent to the outer edge of the contact region (see Fig. 27).

With driving current $I = 4\,\text{mA}$ it is possible to produce a index variation of $\Delta n = 5.0 \times 10^{-3}$, which for an active region length of 500 μm allows to generate a π phase shift. Switching characteristics are limited by the rise

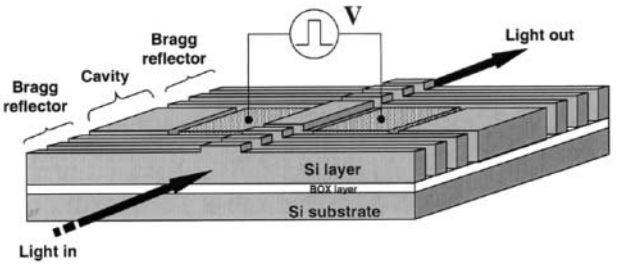

Fig. 28. Sketch of the modulator proposed by *Barrios* et al. [62]

time, which is about 30 ns long. Finally, it is interesting to mention a recent paper by *Barrios* et al. [62], where the authors perform an accurate theoretical analysis of a Fabry–Perot modulator with deep Si/SiO_2 Bragg reflectors (see Fig. 28).

Carriers are also laterally confined in the cavity region by employing deep-etched trenches. The refractive index of the cavity is varied by using the free-carrier dispersion effect produced by a p–i–n diode. The device has been designed and analyzed using electrical and optical simulations. Their calculations predict, for a 20-μm-long device, a modulation depth of around 80% and a transmittance of 86% at an operating wavelength of 1.55 μm by using an electrical power under dc conditions on the order of 25 μW. The switching speed of this device is calculated to be about 16 ns.

References

1. R. A. Soref: Silicon-based optoelectronics, Proc. IEEE **81**, 1687–1706 (1993)
2. G. Breglio, A. Cutolo, A. Irace, P. Spirito, L. Zeni, M. Iodice, P. Sarro: Two silicon optical modulators realizable with a fully compatible bipolar process, IEEE J. Sel. Top. Quantum Electron. **4**, 1003–1010 (1998)
3. R. A. Soref, J. P. Lorenzo: Single-crystal silicon-A new material for 1.3 and 1.6 μm integrated-optical components, Electron. Lett. **21**, 953–955 1985
4. G. Cocorullo, F. D. Corte, I. Rendina, A. Cutolo: New possibilities for efficient silicon integrated electro-optical modulators, Opt. Commun. **86**, 228–235 (1991)
5. R. A. Soref, B. R. Bennett: Electrooptical effect in Silicon, IEEE J. Quantum Electron. **QE-23**, 123–129 1987
6. P. H. Wendland, M. Chester: Electric field effects on indirectoptical transitions in silicon, Phys. Rev. **140**, 1384 (1965)
7. T. S. Moss, G. J. Burrell, B. Ellis: *Semiconductor Opto-Electronics*, (Butterworths, London 1975)
8. P. E. Schmid: Optical absorption in heavily doped silicon, Phys. Rev. B **23**, 5531 (1981)
9. A. A. Volfson, V. K. Subashiev: Fundamental absorption edgeof silicon heavily doped with donor or acceptor impurities, Sov. Phys. Semicond. **1**, 327–332 (1967)

10. W. Spitzer, H. Y. Fan: Infrared absorption in n-type silicon, Phys. Rev. **108**, 268 (1957)
11. W. C. Dash, R. Newman: Intrinsic optical absorption in single-crystal germanium and silicon, Phys. Rev. **99**, 1151–1155 (1955)
12. M. Balkanski, J. M. Besson: Optical properties of degenerate silicon, Tech. Note 2, Contract AF61(052)-789, Defense Tech. In-form. Cen., AD 619581 (1965)
13. C. M. Randall, R. D. Rawcliffe: Refractive indices of germanium, silicon, and fused quartz in the far infrared, Appl. Optics, **6**, 1889 (1967)
14. P. A. Schumann Jr., W. A. Keenan, A. H. Tong, H. H. Gegenwarth, C. P. Schneider: Optical constants of silicon in the wavelength range 2.5 to 40 μm, IBM Tech. Rep. TR-22.1008, East Fishkill,NY , May 20 (1970)
15. S. Walles: Transmission of silicon between 40 and 100 μm, ArkivFysik, **25**, 33 (1964)
16. S. Walles, S. Boija: Transmittance of doped silicon between 40and 100 μm, J. Opt. Soc. Amer. **54**, 133–134 (1964)
17. P. A. Schumann, R. P. Phillips: Comparison of classical approximation to free carrier absorption in semiconductors, Solid State Electron. **10**, 943 (1967)
18. P. Lautenschlager, M. Garriga, L.Viña, M. Cardona: Temperature dependence of the dielectric function and interband critical points in silicon, Phys. Rev. B, **36**, 4821 (1987)
19. M. R. Siregar, M. von Allmen, W. Luthy: Temperature Dependence of Optical Absorption at 1.06 μm in Amorphous and Crystalline Silicon, Rapport de la session d'automne de la Société Suisse de Physique **52**, 45 (1979)
20. H. H. Li: Refractive Index of Silicon and Germanium and Its Wavelength and Temperature Derivatives, J. Phys. Chem. Ref. Data **9**, 561 (1980)
21. G. E. Jellison, Jr., H. H. Burke: The temperature dependence of the refractive index of silicon at elevated temperatures at several laser wavelengths, J. Appl. Phys. **60**, 841 (1986)
22. M. Bertolotti, V. Bogdanov, A. Ferrari, A. Jascow, N. Nazarova, A. Pikhtin, L. Schirone: Temperature dependence of the refractive index in semiconductors, J. Opt. Soc. Am. B, **7**, 918 (1990)
23. G. Ghosh: Temperature dispersion of refractive indices in crystalline and amorphous silicon, Appl. Phys. Lett. **66**, 3570 (1995)
24. N. A. Nazarova, G. I. Romanova, A. D. Yaskov: Refractometric characteristics of silicon, Sov. J. Opt. Technol. **55**, 220 (1988)
25. G. Cocorullo, I. Rendina: Thermo-optical modulation at 1.5 μm in silicon etalon, Electron. Lett. **28**, 83 (1992)
26. G. Cocorullo, F. G. Della Corte, I. Rendina: Temperature dependence of the thermo-optic coefficient in crystalline silicon between room temperature and 550 K at the wavelength of 1523 nm, Appl. Phys. Lett. **74**, 3338 (1999)
27. F. G. Della Corte, M. Esposito Montefusco, L. Moretti, I. Rendina, G. Cocorullo: Temperature Dependence Analysis of the Thermo-Optic Effect in Silicon by Single and Double Oscillator Models, J. Appl. Phys. **88**, 7115 (2000)
28. A. N. Pikhtin, A. D. Yaskov: Dispersion of refractive index of semiconductor with diamond and zinc-blende structures, Sov. Phys. Semicond. **12**, 622 (1978)
29. I. M. Grodnenskiy, I. N. Dyuzhikov, I. O. Ogloblin, Y. F. Sokolov, K. V. Starostin: The use of silicon p–i–n structures for controlling radiation with a wavelength of 1.15 μm, Radio Eng. Electron. Phys. **26**, 147 (1981)

30. D. F. Clark, D. Uttamchandani, I. Andonovic, B. Culshaw: Optical waveguides in silicon for optical interconnects, Optical Interconnects, IEE Colloquium (1988), pp. 12/1–12/61
31. S. P. Pogossian, L. Vescan, A. Vonsovici: The single-mode condition for semiconductor rib waveguides with large cross section, J. Lightwave Technol. **16**, 1851–1853 (1998)
32. G. Cocorullo, F. G. Della Corte, M. Iodice, T. Polichetti, I. Rendina, P. M. Sarro: Low Loss All-Silicon Single Mode Optical Waveguide with Small Cross-Section, Fiber and Integrated Optics, **20**, 207–219 (2001)
33. R. A. Soref, J. P. Lorenzo: All-silicon active and passive guided-wave components for $\lambda = 1.3$ and 1.6 μm, IEEE J. Quantum Electron. **QE-22**, 873–879 (1986)
34. J. P. Lorenzo, R. A. Soref: 1.3 μm electro-optic silicon switch, Appl. Phys. Lett. **51**, 6 (1987)
35. G. V. Treyz, P. G. May, J. M. Halbout: Silicon optical modulators at 1.3 μm based on free-carrier absorption, Electron. Dev. Lett. **12**, 276–278 (1991)
36. O. Leistiko, H. Bak: Planar silicon optical waveguide light modulators, 24th European Solid State Device Research Conference, Edinburgh, Scotland (1994), pp. 645–648
37. A. Cutolo, M. Iodice, P. Spirito, L. Zeni: Silicon Electro-Optic Modulator Based on a Three Terminal Device Integrated in a Low-Loss Single-Mode SOI waveguide, J. Lightwave Technol. **15**, 505 (1997)
38. A. Sciuto, S. Libertino, A. Alessandria, S. Coffa, G. Coppola: Design, fabrication, and testing of an integrated Si-based light modulator, J. Lightwave Technol. **21**, 228–235 (2003)
39. C. Z. Zhao, E. K. Liu, G. Z. Li, L. Gu: Silicon-on-insulator optical intensity modulator based on waveguide-vanishing effect, Electron. Lett. **32**, 1667–1668 (1996)
40. B. R. Hemenway, O. Solgaard, D. M. Bloom: All-silicon integrated optical modulator for 1.3 μm fiber-optic interconnects, Appl. Phys. Lett. **55**, 349 (1989)
41. G. V. Treyz, P. G. May, J. M. Halbout: Silicon Mach–Zehnder waveguide interferometers based on the plasma dispersion effect, Appl. Phys. Lett. **59**, 771 (1991)
42. X. Xiao, J. C. Sturm, K. K. Goel, P. V. Schwartz: Fabry–Perot optical intensity modulator at 1.3 μm in silicon, Photon. Technol. Lett. **3**, 230 (1991)
43. Y. M. Liu, X. Xiao, P. R. Prucnal, J. C. Sturm: All-optical switching in an asymmetric Fabry-Perot étalon based on the free-carrier plasma effect, Appl. Opt. **33**, 3871 (1994)
44. G. Cocorullo, M. Iodice, I. Rendina: All-silicon Fabry-Perot modulator based on the thermo-optic effect, Opt. Lett. **19**, 420 (1994)
45. G. Cocorullo, M. Iodice, I. Rendina, P. M. Sarro: Silicon thermooptical micromodulator with 700-kHz −3-dB bandwidth, Photon. Technol. Lett. **7**, 363 (1995)
46. M. Iodice, F. G. Della Corte, I. Rendina, P. M. Sarro, M. Bellucci: Transient analysis of a high-speed thermo-optic modulator integrated in an all-silicon waveguide, Opt. Eng. **42**, 169 (2003)
47. L. Friedman, R. A. Soref, J. P. Lorenzo: Silicon double-injection electro-optic modulator with junction gate control, J. Appl. Phys. **63**, 1831 (1988)
48. G. V. Treyz: Silicon Mach–Zehnder waveguide interferometers operating at 1.3 μm, Electron. Lett. **27**, 118 (1991)

49. C. K. Tang, G. T. Reed: Highly efficient optical phase modulator in SOI waveguides, Electron. Lett. **31**, 451 (1995)
50. C. Z. Zhao, G. Z. Li, E. K. Liu, Y. Gao, X. D. Liu: Silicon on insulator Mach–Zehnder waveguide interferometers operating at 1.3 μm, Appl. Phys. Lett. **67**, 2448 (1995)
51. P. Dainesi, A.Küng, M. Chabloz, A. Lagos, Ph. Flückiger, A. Ionescu, P. Fazan, M. Declerq, Ph. Renaud, Ph. Robert: CMOS compatible fully integrated Mach–Zehnder interferometer in SOI technology, Photon. Technol. Lett. **12**, 660 (2000)
52. S. R. Giguere, L. Friedman, R. A. Soref, J. P. Lorenzo: Simulation studies of silicon electro-optic waveguide devices, J. Appl. Phys. **68**, 4964 (1990)
53. H. C. Huang, T. C. Lo: Simulation and analysis of silicon electro-optic modulators utilizing the carrier-dispersion effect and impact-ionization mechanism, J. Appl. Phys. **74**, 1521 (1993)
54. C. K. Tang, G. T. Reed, A. J. Walton, A. G. Rickman: Low-loss, single-mode, optical phase modulator in SIMOX material, J. Lightwave Technol. **12**, 1394–1400 (1994)
55. C. C. Wang, M. Currie, S. Alexandrou, T. Y. Hsiang: Ultrafast, all-silicon light modulator, Optics Lett. **19**, 1453 (1994)
56. M. Y. Liu, S. Y. Chou: High-modulation-depth and short-cavity-length silicon Fabry–Perot modulator with two grating Bragg reflectors, Appl. Phys. Lett. **68**, 170 (1996)
57. A. Cutolo, M. Iodice, A. Irace, P. Spirito, L. Zeni: An electrically controlled Bragg reflector integrated in a rib silicon on insulator waveguide, Appl. Phys. Lett. **71**, 199 (1997)
58. A. Vonsovici, R. Orobtchouk, A. Koster: Numerical simulation of a silicon-on-insulator waveguide Fabry–Perot interferometer for intensity light modulators at 1.3 μm, J. Lightwave Technol. **15**, 2124 (1997)
59. G. Coppola, A. Irace, M. Iodice, A. Cutolo: Simulation and analysis of a high-efficiency silicon optoelectronic modulator based on a Bragg mirror, Opt. Eng. **40**, 1076 (2001)
60. A. Irace, G. Breglio, A. Cutolo: All-silicon optoelectronic modulator with 1 GHz switching capability, Electron. Lett. **39**, 232 (2003)
61. P. D. Hewitt, G. T. Reed: Improved modulation performance of a silicon p–i–n device by trench isolation, J. Lightwave Technol. **19**, 387 (2001)
62. C. A. Barrios, V. Rosa de Almeida, M. Lipson: Low-power-consumption short-length and high-modulation-depth silicon electrooptic modulator, J. Lightwave Technol. **21**, 1089–1098 (2003)

Index